Article

JOURNAL OF COMPOSITE MATERIALS

Journal of Composite Materials
46(11) 1323–1334

DOI: 10.1177/0021998311418262
jcm.sagepub.com

SAGE

Evaluation of strength-controlling defects in paper by stress concentration analyses*

John M Considine[1], David W Vahey[1], James W Evans[1], Kevin T Turner[2] and Robert E Rowlands[2]

Abstract

Cellulosic webs, such as paper materials, are composed of an interwoven, bonded network of cellulose fibers. Strength-controlling parameters in these webs are influenced by constituent fibers and method of processing and manufacture. Instead of estimating the effect on tensile strength of each processing/manufacturing variable, this study modifies and compares the point stress criteria and average stress criteria models used to estimate defect-free (i.e., maximum possible) tensile strength and the inherent size of the cumulative effect of strength-limiting defects. The two major modifications to these models were to assume that defect-free tensile strength was unknown and that unnotched tensile strength was reduced by the presence of inherent defects. These modifications allow the calculation of inherent defect size and defect-free tensile strength by characterizing the tensile strength of the web in the presence of stress concentrations associated with holes of different radius. The models were applied to seven paper materials including lightweight, commercial papers, linerboards, and cylinder boards; estimated inherent defect sizes ranged from 0.1 to 1.5 mm. For most materials considered, defect size was larger in the 2-direction than the 1-direction. Actual measured tensile strengths ranged from 59% to over 95% of the estimated defect-free tensile strengths, σ_u.

Keywords

paper, paper strength, tensile strength, defects, defect size, formation, notched specimens, unnotched strength, stress distribution, point stress criterion, average stress criterion, nonlinear least squares

Introduction

Paper materials are three-dimensional (3D) networks of cellulose fibers. Primary variables that contribute to a well-made paper sheet are pulp fiber properties, grammage (mass/unit area), density, drying restraint, and fiber orientation. However, each of these variables has microscopic spatial gradients that contribute to local and global behaviors. The ability to relate these variables and their gradients to the mechanical behavior of paper may offer opportunities to improve its mechanical performance and therefore increase the use of paper as a structural material.

Deterministic and probabilistic models become unduly complicated when trying to evaluate parameters contributing to the mechanical behavior of cellulosic webs. Examples of these types of models are given in references.[1–3]

Figure 1(a) and (b) shows an example of fiber configuration and alignment within a linerboard sample. It is not feasible to determine from such figures a single critical defect (i.e., a defect that controls web strength). Fibers in these figures have a range of lengths and widths but tend to lie within planes. The 3D nature of paper materials seen in the cross-sectional view of Figure 1(b) illustrates how defects may be present within the material but not visible in planar views.

It is proposed that cellulose webs behave as a conglomeration of defects, interconnected with fibers, which themselves contain defects. Physical

[1]USDA Forest Service, Forest Products Laboratory, One Gifford Pinchot Drive, Madison, WI 53726, USA
[2]Department of Mechanical Engineering, University of Wisconsin-Madison, Madison, WI 53706, USA

Corresponding author:
John M Considine, USDA Forest Service, Forest Products Laboratory, One Gifford Pinchot Drive, Madison, WI 53726, USA
Email: jconsidine@fs.fed.us

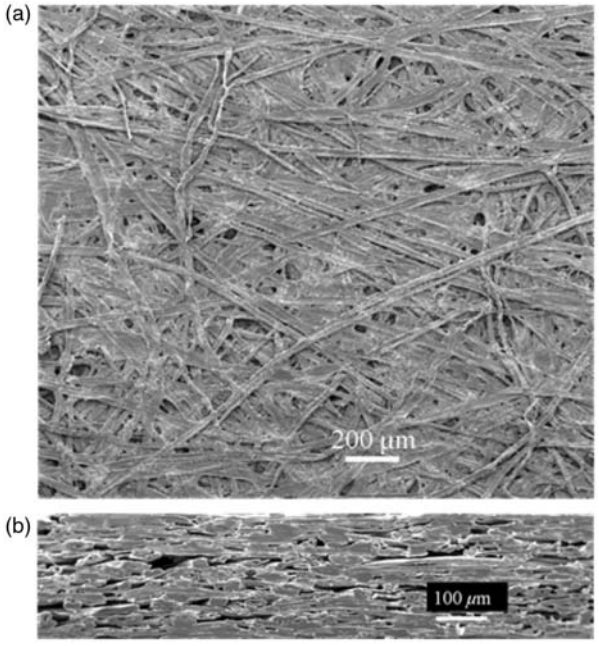

Figure 1. SEM images of a linerboard: (a) surface and (b) cross-section view.

identification of size and location of a single strength-controlling defect is not possible; however, these materials behave as though their failure is associated with an effective defect of a particular size. This can occur even if no defects of that physical size exist within the structure. Such an entity will be called an 'inherent defect.' Moreover, the tensile strength of a material with a size '0' inherent defect will be defined as the 'maximum potential tensile strength' and denoted by σ_u.

Researchers have previously tried to relate measured tensile strength, a macroscopic property, to local mass variation, or formation, but no clear picture has emerged. Table 1, containing[4–10] summarizes many of these more significant contributions. Regardless of pulping method, fiber type, or forming method, researchers have found a variety of relationships.

Using laboratory handsheets, I'Anson and Sampson[11] found a relationship between fiber dimensions, sheet grammage, and specific tensile strength, such that a maximum specific tensile strength occurred near a grammage of 50 g/m^2, which is less than that of most printing and writing papers. In terms of the present models, fiber dimensions, bonding, and material thickness might coalesce at this grammage level to produce an inherent defect size smaller, thereby increasing strength, than at either larger or smaller grammages. The models are comparable to the use of the critical flaw size in statistical fracture mechanics to describe the transition between a disorder-dominated size-dependent material and one that can be described by linear elastic fracture mechanics.[12]

Natural defects in poorly formed sheets increase strain disorder[13] and cause separate regions that exhibit elastic and plastic response to occur simultaneously under uniform global stress. A continuum model developed by Korteoja *et al.*[14] indicates that large strain variations within a sheet reduce tensile strength. Researchers have mapped full-field displacements of tensile-loaded paper and paperboard using digital image correlation (DIC) to characterize variations in strain.[15–18] These mappings showed large strain variations even in papers with apparently good formation, suggesting the existence of stress concentrators. DIC demonstrated large strains near low-grammage regions or holes. In particular, Wong *et al.*[17] found that local grammage and local tensile strain are inversely proportional to each other. Considine *et al.*[18] observed compressive strain near low-grammage regions of tensile specimens and attributed those strains to low-modulus inclusions.

Scale of measurement is an important aspect of evaluating behavior of materials composed of cellulose fibers. Hristopulos and Uesaka[19] examined the strength distribution in newsprint and suggested that the critical cluster was on the order of a millimeter, where the critical cluster is defined as the strength-controlling size in weak-link modeling. Other researchers[20] have suggested a larger value based on floc size. Flocs are small regions of higher grammage than the sheet average and are balanced by corresponding low-grammage regions. Floc size, grammage variation, and local fiber orientation each contribute to strength behavior.[21]

The present research is similar to that of Rhee *et al.*[22], who introduced multiple holes in a tensile specimen in order to examine changes in strength caused by defects and stress interaction. Stress distributions associated with individual neighboring holes in a tensile specimen tended to interact with each other and modify the stress concentration factor for any single hole. The present investigation assumes that an introduced defect will interact with physical defects created during manufacturing. Two paper sheets with poor formation in the form of low-modulus inclusions in a high-modulus matrix can have widely differing strengths, suggesting that formation alone is not a strength-determining factor. Recognizing this, the present investigation extends the work of Um and Perkins[16] and Perkins and Um,[23] who measured strains in the vicinity of a single hole in a tensile paper strip, calculated associated stresses, and compared their measurements with finite element analysis to show hole boundary stresses greater than the material's tensile strength. Using a quasi-isotropic point stress criterion (PSC), researchers have predicted tensile strengths of paper specimens with a single hole.[23,24]

Table 1. Summary of previous work relating tensile strength to formation

Reference	Pulp–Fiber	Sheet forming	Finding
Norman[4]	Chemical – hardwood and softwood	Handsheet (isotropic)	Direct relationship between tensile strength loss and large variation of local mass
Moffatt *et al.*[5]	Mechanical – hardwood	Machine made (orthotropic)	Failure zone passes through regions of low grammage
Nazhad *et al.*[6,7]	Mechanical – softwood Chemical – hardwood	Handsheet	Direct relationship between tensile strength loss and formation
Mohlin[8]	Hardwood and softwood	Machine made	No relationship between strength and formation
Nordstrom[9]	Chemical – softwood	Machine made	Relationship between tensile strength and formation depends on grammage and fiber bonding
Wathen and Niskanen[10]	Mechanical and chemical – hardwood	Machine made	Weak correlation between tensile strength and formation

Table 2. Physical and mechanical properties of materials examined

	50% RH properties of designated materials						
Property	C	E	F	L1	L2	S1	S2
Grammage (g/m^2)	76	92	187	268	209	261	258
Thickness (mm)	0.11	0.13	0.31	0.38	0.30	0.40	0.40
Density (kg/m^3)	721	734	603	717	688	648	643
E_{11} (GPa)	7.82	7.38	4.52	7.80	7.75	9.40	8.20
E_{22} (GPa)	2.56	3.40	2.12	3.71	3.73	2.22	2.02
G_{12} (GPa)	1.63	1.85	1.27	2.10	2.15	0.71	0.70
ν_{12}	0.17	0.23	0.18	0.20	0.23	0.18	0.19
E_{11}/E_{22}	3.05	2.20	2.13	2.10	2.08	4.27	4.06

Note: C, copy; E, envelope; F, filter; L1, linerboard1; L2, linerboard2; S1, cylinder board1; and S2, cylinder board2.

The present approach is designed to evaluate macroscopic differences in papers due to widespread, mesoscopic defects. The presence of flaws, defined as one-time or occasional defects, is not addressed. Additionally, this approach is based on stress concentration analysis as opposed to stress intensity analysis used in fracture mechanics models. Failure is assumed to be caused by inherent defects that are larger than a critical defect.

Materials and methods

Defect analyses are investigated here on seven commercially available cellulosic materials whose physical and mechanical properties are listed in Table 2. Sheet thickness was measured with a Mitutoyo® (Kawasaki, Japan) 543-396B Digital Indicator equipped with a ball tip of diameter 4 mm. Elastic moduli and Poisson's ratios were obtained ultrasonically with a Nomura Shoji Corporation (Tokyo, Japan) Sonic Sheet Tester (SST). The SST is equipped with one sensor pair, which operates at 25 kHz; measurements were taken at 5° intervals by rotating the sample on a turntable.

Material C is a commercial copy paper containing about 8% ash. Material E is a commercial bond envelope paper and likely contains cotton fibers. Material F is a commercial filter paper manufactured by Whatman® International (Maidstone, Kent, UK), identified as Chromotography Paper, Model 3MM CHR, and was chosen because it is 100% cellulose from cotton linters. Material L1 is a commercial linerboard whose fiber content likely contains both virgin

and recycled fibers. Material L2, made on a different machine than L1, is an unbleached, kraft single-ply linerboard, and like L1, a material commonly used in structural paperboard products such as corrugated containers. Materials S1 and S2 are cylinder boards made on the same cylinder machine but with a proprietary processing change between materials.

The material properties in Table 2 represent a broad spectrum of paper and paperboards. The density range indicated is fairly typical. Recognizing that the density of native cellulose is approximately 1500 kg/m^3 indicates these papers have a large amount of void space. The orthotropy ratio, E_{11}/E_{22}, may be as high as 5:1 for specially manufactured paperboards, but low ratios, about 2:1, are typical for structural paperboards.

Tensile testing

Tensile tests were performed on an Instron® (Norwood, Massachusetts) Model 5865 test machine equipped with line-clamp pneumatic grips. Gage length, which was determined by available material sizes, was 200 mm for materials S1 and S2 and 125 mm for all other materials. Width was 25 mm. The test sequence started with a pre-load to 1 N at 12 N/min, followed by displacement at a constant speed of 1.5 mm/min that continued to specimen failure. Load and grip displacement data were collected at 10 Hz. All tests were performed in a controlled environment at 50% relative humidity (RH) and 23°C.

Some samples were susceptible to tensile buckling; curvature would occur across the specimen width. This was avoided and test similarity insured by transversely restraining all specimens with glass plates. This was accomplished by positioning the specimens between two 100 mm long restraining glass plates separated by a gap of twice the sample thickness and placed at the vertical center of the tensile specimen. These plates were held independent of the test machine and were stationary during tensile testing.

Specimen preparation

Figure 2 shows the basic specimen geometry. Each specimen contained a single hole prepared with specially designed tool steel machined punches that have an inner cutting taper to prevent densification of the material near the hole boundary. Holes were located with alignment fixtures that consisted of a different specific fixture for each specimen geometry. The alignment fixtures insured hole location along the longitudinal centerline and held the specimen firmly to a backing plate during the cutting process. Individual specimens each had a single hole of radius 0.25, 1.25, 1.88, 2.5, or 5.0 mm, and five tensile test replications for each sample were performed.

Evaluation of inherent defect size and potential strength

All cellulosic webs contain inherent defects, whether due to poor formation, fiber damage, or non-uniform fiber bonding. The goal of this research was to determine an inherent defect size and a maximum potential tensile strength, σ_u, for paper materials. Maximum potential tensile strength is the tensile strength of defect-free material, but made with the same fibers, processing, bonding, and orthotropic properties as the web under inspection. Inherent defect size, R_{eff}, is determined by comparing the behavior of the sample material to that of models that estimate the effect of defect size.

Model development

Awerbuch and Madhukar[25] reviewed many semi-empirical strength models and concluded that each model could adequately represent the data so long as the empirical parameters were accurately determined. The PSC and average stress criterion (ASC), both created by Whitney and Nuismer[26], are modified here and applied to measured strength data of seven paper materials in Table 2. Modification of these models includes correction for finite-width specimens, assumption that defect-free tensile strength is unknown, and use of unnotched tensile strength to determine inherent

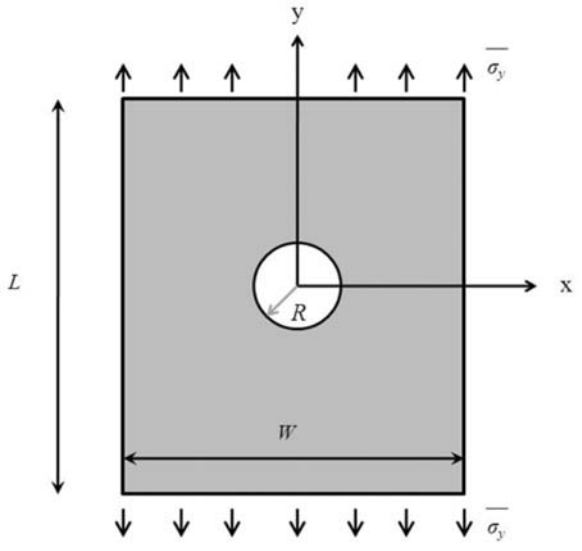

Figure 2. Schematic of specimen. $L = 125$ or 200 mm, $W = 25$ mm, and $R = 0.25$, 1.25, 1.88, 2.5, or 5.0 mm.

defect size. The development of the modified PSC and ASC models follows.

For an infinite uniaxially loaded, linear elastic, orthotropic sheet containing a central circular hole of radius R (Figure 2), the tensile stress along the y-axis, beginning at the edge of the hole, $\sigma_y^{\infty}(x,0)$, $x \geq R$, is given by Lekhnitskii[27] as

$$\sigma_y^{\infty}(x,0) = \overline{\sigma_y} + \overline{\sigma_y}\mathrm{Re}\left\{\frac{1}{\mu_1-\mu_2}\left[\frac{-\mu_2(1-i\mu_1)}{\sqrt{\gamma^2-1-\mu_1^2\left(\gamma+\sqrt{\gamma^2-1-\mu_1^2}\right)}} + \frac{\mu_1(1-i\mu_2)}{\sqrt{\gamma^2-1-\mu_2^2\left(\gamma+\sqrt{\gamma^2-1-\mu_2^2}\right)}}\right]\right\} \quad (1)$$

where Re denotes the real part of the expression in the brackets, $\overline{\sigma_y}$ the far-field applied stress ($y \to \pm\infty$), $\gamma = x/R$, and μ_1 and μ_2 the two solutions of the following equation (μ_3 and μ_4 are complex conjugates of μ_1 and μ_2):

$$a_{22}\mu^4 - 2a_{26}\mu^3 + (2a_{12}+a_{66})\mu^2 - 2a_{16}\mu + a_{11} = 0 \quad (2)$$

In Equation (2), a_{ij}, $i,j = 1,2,6$, are compliances of the orthotropic material. In the present case, $a_{16} = a_{26} = 0$, and

$$\begin{bmatrix} a_{11} & a_{12} & a_{16} \\ \cdot & a_{22} & a_{26} \\ \cdot & \cdot & a_{66} \end{bmatrix} = \begin{bmatrix} \frac{1}{E_{11}} & -\frac{\nu_{12}}{E_{11}} & 0 \\ \cdot & \frac{1}{E_{22}} & 0 \\ \cdot & \cdot & \frac{1}{G_{12}} \end{bmatrix} \quad (3)$$

Complex material properties μ_i depend on E_{11}, E_{22}, ν_{12}, and G_{12}, where the 1 (MD, machine direction) and 2 (CD, cross-machine direction) directions are the orientations of material symmetry. Procedures for determining μ_i of Equation (2) are readily available[28] and must be determined for each material under consideration.

Using a similar approach to that of Khashaba[29], Tan's[30] finite-width specimen correction factor, FWC, is incorporated to adjust the stress distribution given as

$$\mathrm{FWC} = \frac{K_T}{K_T^{\infty}} \quad \text{and} \quad \frac{K_T}{K_T^{\infty}}\sigma_y^{\infty}(x,0) = \sigma_y(x,0) \quad (4)$$

where K_T and K_T^{∞} are the tensile stress concentration factors at $(x,y) = (R,0)$ for a finite-width and infinite specimens, respectively, of the same material.

Enforcing y-direction equilibrium, for both the infinite width and finite-width specimens, is accomplished by integrating Equation (4), i.e.

$$\frac{RK_T}{K_T^{\infty}}\int_1^{W/2R}\sigma_y^{\infty}(x,0)\mathrm{d}\gamma = \overline{\sigma_y}\cdot W/2 \quad (5)$$

This force equilibrium causes the FWC to uniformly increase the stress magnitude; Equation (4) assumes the same general stress profile along the x-axis from the hole for both an infinite- and finite-width geometries. Combining Equations (1) and (4) at $x = R$ gives

$$\frac{1}{\mathrm{FWC}} = \frac{K_T^{\infty}}{K_T} = 1 - \frac{2R}{W} + \mathrm{Re}\left\{\frac{1}{\mu_1-\mu_2}\left[\frac{\mu_2}{1+i\mu_1}\left(1-\frac{2R}{W}-i\mu_1\left(\frac{2R}{W}\right)\right.\right.\right.$$
$$\left.\left.\left. - \sqrt{1-\left(1+\mu_1^2\right)\left(\frac{2R}{W}\right)^2}\right) - \frac{\mu_1}{1+i\mu_2}\left(1-\frac{2R}{W}-i\mu_2\left(\frac{2R}{W}\right)\right.\right.\right.$$
$$\left.\left.\left. - \sqrt{1-\left(1+\mu_2^2\right)\left(\frac{2R}{W}\right)^2}\right)\right]\right\} \quad (6)$$

where W is the specimen width.

The PSC states that a tensile sheet containing a central circular hole of radius, R, fails when the longitudinal stress, σ_y, at a characteristic distance, d_0, from the edge of the hole achieves the unnotched tensile strength of the material in the y-direction, σ_U (i.e., failure occurs when $\sigma_y(R+d_0,0) = \sigma_U$). Alternatively stated, failure occurs when the longitudinal stress throughout the distance adjacent to the edge of the hole, d_0, exceeds the unnotched tensile strength, σ_U.

In the foregoing discussion, the unnotched tensile strength σ_U is the strength of the material as determined by a conventional tensile test. Quantity, σ_u (note lowercase subscript), is considered an unknown parameter. It is associated with processing defects and is to be determined via nonlinear least squares regression of the equation that results when σ_u is set equal to the product of Equation (1) and the reciprocal of Equation (6). Moreover, $\gamma_0 = (R+d_0)/R$, and μ_1 and μ_2 are the principal roots of Equation (2). To denote this change, the subscripts are changed such

that $\sigma_U \to \sigma_u$. The resulting PSC as modified for a hole in a finite-width orthotropic plate is

$$\sigma_u = \mathrm{FWC} \cdot \sigma_H \left\{ 1 + \mathrm{Re}\left\{ \frac{1}{\mu_1 - \mu_2} \left[\frac{-\mu_2(1 - i\mu_1)}{\sqrt{\gamma_0^2 - 1 - \mu_1^2\left(\gamma_0 + \sqrt{\gamma_0^2 - 1 - \mu_1^2}\right)}} + \frac{\mu_1(1 - i\mu_2)}{\sqrt{\gamma_0^2 - 1 - \mu_2^2\left(\gamma_0 + \sqrt{\gamma_0^2 - 1 - \mu_2^2}\right)}} \right] \right\} \right\} \tag{7}$$

where σ_H is the experimentally measured tensile strength of the notched specimens and σ_u and γ_0 (i.e., d_0) are unknowns.

A related criterion to the PSC, using the same geometry, is the ASC, which assumes failure will occur when the average longitudinal stress over a distance, a_0, reaches the unnotched tensile strength of the material in the y-direction, σ_U (i.e., failure occurs when $\sigma_U = (1/a_0)\int_R^{R+a_0} \sigma_y(x,0)\mathrm{d}x$)[26]. The ASC, as modified for the present finite-width specimens, can be formally written as

$$\sigma_u = \frac{\mathrm{FWC} \cdot \sigma_H}{a_0} \int_R^{R+a_0} \left\{ 1 + \mathrm{Re}\left\{ \frac{1}{\mu_1 - \mu_2} \left[\frac{-\mu_2(1 - i\mu_1)}{\sqrt{\gamma^2 - 1 - \mu_1^2\left(\gamma + \sqrt{\gamma^2 - 1 - \mu_1^2}\right)}} + \frac{\mu_1(1 - i\mu_2)}{\sqrt{\gamma^2 - 1 - \mu_2^2\left(\gamma + \sqrt{\gamma^2 - 1 - \mu_2^2}\right)}} \right] \right\} \right\} \mathrm{d}x \tag{8}$$

The strictly linear elastic PSC solution has been applied to nonlinear materials by many researchers including Kortschot and Trakas[24] and Perkins and Um[23], who both applied a quasi-isotropic PSC to paper; by Khashaba[29], who applied a modified PSC to a glass fiber reinforced polyester material; and by McNulty *et al.*[31], who applied PSC to Nicalon-reinforced ceramic composites. Significantly more applications have been made of the PSC than of the computationally more difficult ASC.

Numerical analysis

Unknown parameters, σ_u and d_0 for Equation (7) and σ_u and a_0 for Equation (8), were determined by nonlinear least squares regression analysis within Matlab® via the built-in *nlinfit* function. Equation (7) was sensitive to initial estimates for the unknowns due to multiple local minima for these data. For the modified PSC of Equation (7), parameter convergence was realized when a ±10% change in the initial estimates converged to the same values. Equation (8) was insensitive to initial estimates and converged rapidly. Integration of Equation (8) was performed by trapezoidal rule. During nonlinear regression, $\sigma_u \geq \sigma_M$ was a condition, where σ_M is the mean unnotched tensile strength.

Results and discussion

The modified PSC (Equation (7)) and modified ASC (Equation (8)) were used to model the tensile behavior of specimens containing a single hole and for specimens that failed at the hole. Some combinations of material, orthotropic direction, and hole size did not fail at the prepared hole. These specimens were not included in the analysis and will be discussed separately. Inherent defect size was determined by reverse correlation as the intersection of σ_M with the modified PSC or ASC curves.

Figures 3–9 show the results of fitting the modified PSC and ASC curves to single hole tensile data. For the models, the modified PSC is represented by the dark line and the modified ASC by the gray line. Solid squares and circles each represent the measured tensile strength of a specimen when failure occurred away from the introduced hole. Open squares and circles each represent the measured tensile strength of a specimen when failure occurred at the introduced hole. The upper (squares) and lower (circles) sets of data for each graph are for testing in the one- and two-directions, respectively. Papermakers define the 1-direction as the machine direction (denoted by MD) and the 2-direction as the cross-machine direction (denoted by CD). For specimens loaded in each of the 1- and 2-directions, horizontal dashed lines are drawn at the mean measured unnotched tensile strength σ_M and intersect the model at an abscissa R_{eff}, the inherent defect size. Specimens with holes larger than the inherent defect size are expected to fail at the hole. Specimens with holes smaller than the inherent defect size are expected to fail elsewhere. Exceptions do occur, and these are likely explained by the concept of defect interaction[22]: The presence of the hole may increase local stresses elsewhere in the sheet causing failure away from the hole, even though the hole is larger than R_{eff}. Alternatively, stress variations away from the hole can increase stresses at the hole, producing failure at

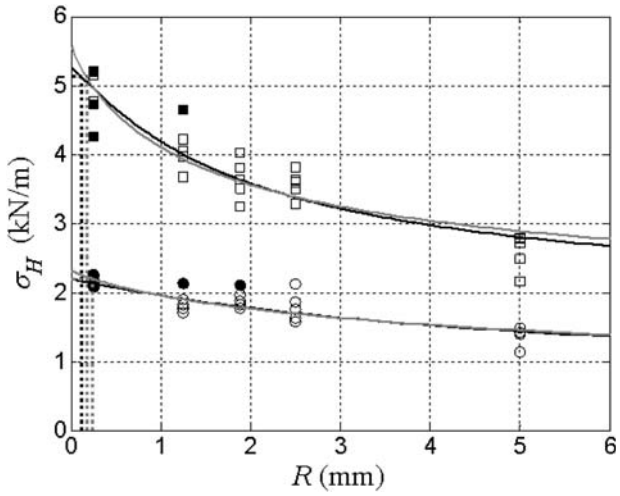

Figure 3. Modified PSC and modified ASC applied to Material C (copy paper) tensile data.

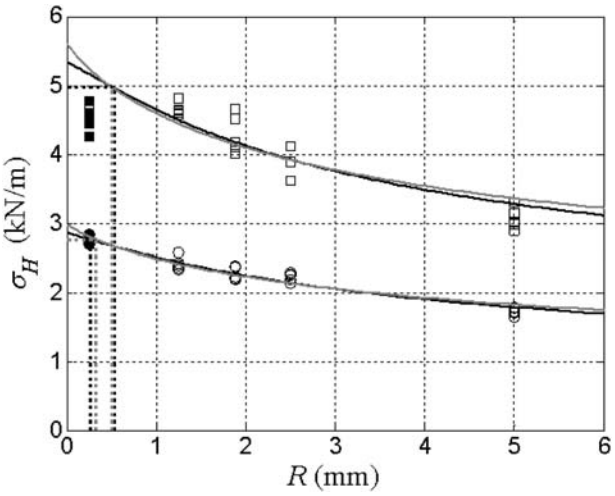

Figure 5. Modified PSC and modified ASC applied to Material F (filter paper) tensile data.

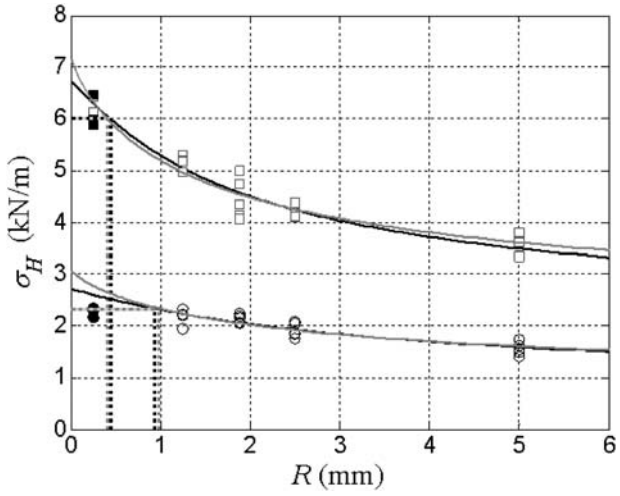

Figure 4. Modified PSC and modified ASC applied to Material E (envelope) tensile data.

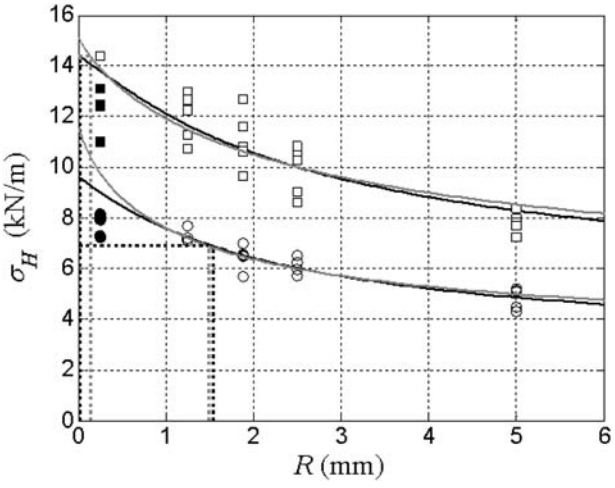

Figure 6. Modified PSC and modified ASC applied to Material L1 (linerboard1) tensile data.

holes smaller than R_{eff}. The models provide an approach for averaging the test data to produce the best indication of R_{eff} regardless of exceptions.

In 9 of 14 cases in Figures 3–9 (seven materials and two directions), the calculated R_{eff} is characterized by tensile failures that avoid holes smaller than R_{eff} and select holes larger than R_{eff}. This is consistent with expectations. For example, Material E, 2-direction in Figure 4, no specimens having the 0.25 mm radius hole failed at the hole, whereas all five specimens with the 1.25 mm radius hole failed at the hole. The calculated R_{eff} (modified ASC) was the intermediate value 0.99 mm. Examining all nine similar cases indicates that the rule followed by Material E, 2-direction, was followed in 78 of the 90 tests of Figures 3–9. The 12 exceptions were likely caused by defect interactions.

In 2 of the 14 cases, Material E for 1-direction (Figure 4) and Material L1 for 2-direction (Figure 6), the calculated R_{eff} is bracketed by hole radii in specimens that failed at the hole. In Material E, 2 of 5 tests failed at 0.25 mm hole, perhaps because of stress enhancement by nearby natural defects. In Material L1, 5 of 5 failures occurred at 1.25 mm holes, when the R_{eff} value (modified ASC) was 1.49 mm. Because the failure percentage of specimens with the smaller hole is 100%, it seems reasonable that strength is likely influenced by cumulative stress interactions among defects along the x-axis such that the introduced hole created a larger than expected defect.

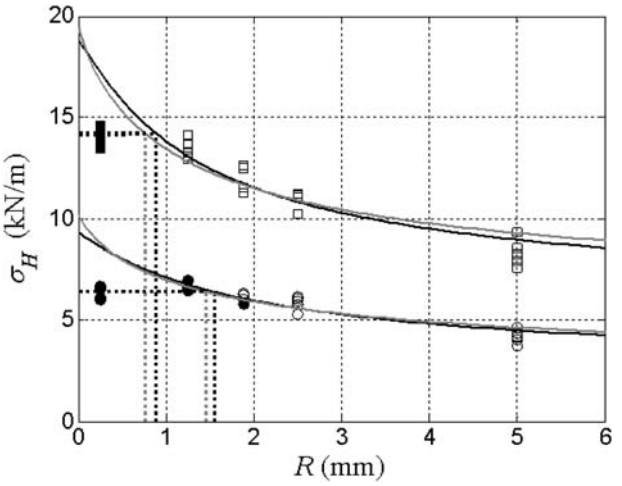

Figure 7. Modified PSC and modified ASC applied to Material L2 (linerboard2) tensile data.

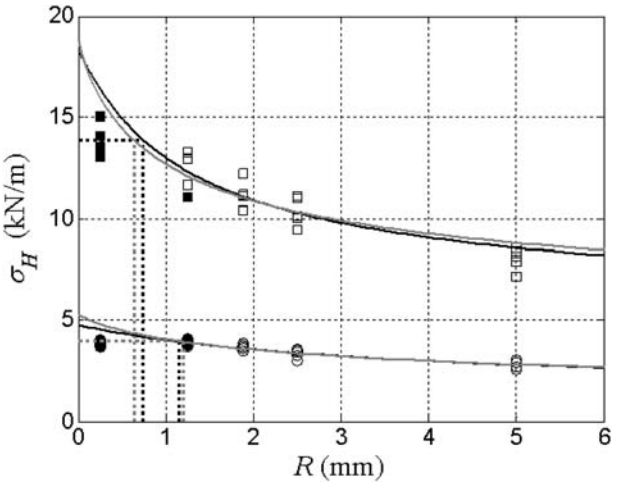

Figure 9. Modified PSC and modified ASC applied to Material S2 (cylinder board2) tensile data.

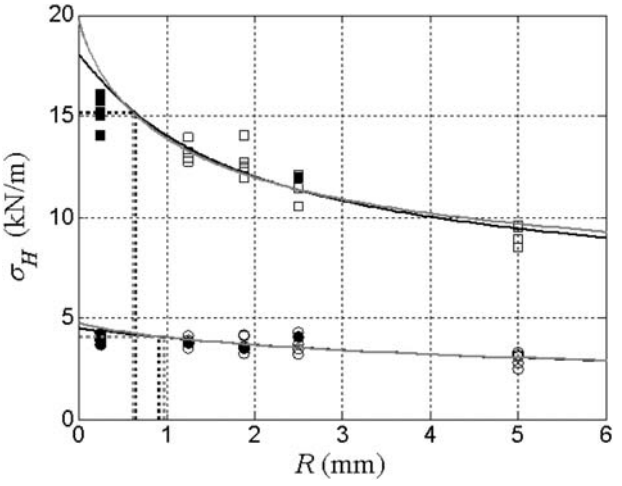

Figure 8. Modified PSC and modified ASC applied to Material S1 (cylinder board1) tensile data.

For the remaining 3 of 14 cases shown in Figures 3–9, R_{eff} is less than 0.25 mm; that is, R_{eff} is less than the radius of the smallest hole used in this study. These cases are Material C in both 1- and 2-directions (Figure 3) and Material L1 in the 1-direction (Figure 6). For these cases, failure should have occurred at 0.25 mm hole. This happened for only 4 of 15 tests. In 11 tests, failure did not occur at the hole, perhaps because of stress shielding by nearby natural defects. This interpretation may be more likely in view of the small size of both the defect and the prepared hole.

Considering all 14 cases in this study, there is the question of defect interaction in 30 of 125 bracketing tests, or 24%. These 30 tests are all limited to specimens where the hole radius was close to R_{eff}. The average absolute discrepancy between R_{eff} and the hole radius is 0.22 mm for R_{eff} evaluated by the PSC model and 0.15 mm for R_{eff} evaluated by the ASC model. These values are influenced by statistical uncertainties in the measurement of σ_{M} for the various specimens. Because the same values of σ_{M} are applied to both the PSC and ASC determination of R_{eff}, the two values are indicative of the relative accuracies of the two models. If, for purposes of discussion, these values are interpreted as absolute accuracies of the two models, the need to go outside the models to explain outliers is greatly reduced. For the ASC model, 17 of the 30 bracketing tests mentioned above are included within the ± 0.15 mm error bars of R_{eff}. Only 13 of 125 bracketing tests remain to defend in terms of defect interactions or otherwise, and 5 of these 13 were limited to material L1 discussed above. For the PSC model, 11 of 30 outlying tests are included within the ± 0.22 mm error bars of R_{eff}, leaving 19 of 125 bracketing tests to defend. Even with smaller error bars (inviting more outliers), the ASC model results in fewer outliers and provides a superior fit to the data. This suggests that the ASC picture of the influence of a hole on tensile strength may capture the physics of failure better than the PSC does, at least in paper samples.

The advantage of the ASC model is further demonstrated by results for Material C, 2-direction (Figure 3). For this sample, the regression limits established give $\sigma_{\text{u}} = \sigma_{\text{M}}$ and $R_{\text{eff}} = 0$ mm for the PSC model. However, according to Table 3, the same cases calculated $\sigma_{\text{u}} > \sigma_{\text{M}}$ and $R_{\text{eff}} > 0$ mm for modified ASC. This suggests that the ASC model may represent a more precise, as well as more accurate, measure of performance.

Both PSC and ASC models are able to differentiate between similar materials in ways that could ultimately prove very useful; for example, consider how the

Table 3. Calculated model parameters

			Point stress			Average stress		
Material	Direction	Measured unnotched strength, σ_M (kN/m)	Calculated unnotched strength, σ_u (kN/m)	$\sigma_M/\sigma_u \times 100\%$	R_{eff} (mm)	Calculated unnotched strength, σ_u (kN/m)	$\sigma_M/\sigma_u \times 100\%$	R_{eff} (mm)
C	1	5.12	5.25	97.4	0.11	5.61	91.3	0.17
	2	2.20	2.20	100.0	0.00	2.33	94.3	0.24
E	1	6.00	6.72	89.4	0.44	7.20	83.3	0.40
	2	2.34	2.72	85.9	0.93	3.09	75.7	0.99
F	1	4.96	5.34	92.9	0.53	5.63	88.2	0.51
	2	2.76	2.86	96.5	0.26	3.00	92.1	0.33
L1	1	14.39	14.41	99.8	0.01	15.20	94.6	0.14
	2	6.88	9.63	71.4	1.53	11.72	58.7	1.49
L2	1	14.20	18.84	75.4	0.88	19.64	72.3	0.76
	2	6.41	9.32	68.8	1.55	10.28	62.4	1.45
S1	1	15.17	18.08	83.9	0.64	19.95	76.1	0.62
	2	4.08	4.51	90.5	0.91	4.80	85.0	0.97
S2	1	13.87	18.30	75.8	0.74	18.97	73.1	0.64
	2	3.94	4.77	82.7	1.15	5.33	74.0	1.20

Note: As in note of Table 2.

models treat similar, high grammage materials: linerboards L1 and L2, and cylinder boards S1 and S2. The exact compositions of materials L1 and L2 are unknown, and they were produced on different paper machines. Nevertheless, Table 2 shows that their densities and ultrasonic mechanical properties are very similar. Only in applying the models are differences made apparent. With R_{eff} close to 0 mm and $\sigma_u \sim \sigma_M$ in the 1-direction, sample L1 (Figure 6) is close to achieving its maximum potential. Though similar in many properties, Sample L2 (Figure 7) has considerable room for improvement in the 1-direction. In the 2-direction, L1 and L2 samples perform somewhat similarly. Both of these cases have room for improvement.

Materials S1 and S2 were manufactured on a cylinder machine, which typically produces a material with discrete layers, very similar to plies in laminated fiber–matrix composites. Additionally, uniform mass distribution is difficult to attain in the cylinder process. As such, these materials add a defect configuration to those present in conventional linerboard papermaking, namely defects between plies.

Figure 8 shows the analysis of Material S1 tensile behavior and illustrates its unique defect configurations. For the 1-direction, all specimens having either a 1.25 or 1.88 mm radius hole failed at these holes, but one of the specimens, which had a 2.5 mm radius hole, failed away from the hole. No other material demonstrated such behavior. The Material S1 in the 2-direction also exhibits some unique behavior in that one specimen of each of those whose hole radius was 1.25, 1.88, or 2.50 mm failed away from the hole. Characterization of an inherent defect size in cylinder-machine papers may not be as important as the demonstration that the material has many defect sizes present.

The supplier of Materials S1 and S2 explained that both materials were made on the same machine but that a proprietary processing change was made to enhance the converting performance of Material S2. Figure 9 shows an application of the models to Material S2 tensile behavior and indicates a more uniform defect configuration than that of Material S1. In the 1-direction of Material S2, only 1 of 15 specimens having a hole of radius larger than R_{eff} failed away from the hole. In the 2-direction of the S2 Material (Figure 9), only one specimen failed at its 1.25 mm hole (close to R_{eff}) and all specimens having holes larger than R_{eff} failed at the holes. Distributions of inherent defect sizes in this material would seem to be narrower than that of Material S1, perhaps indicating improved ply bonding.

Table 3 summarizes results of the analysis. The calculated unnotched strength σ_u is considered to be the maximum potential tensile strength in a defect-free material made with the same fibers and corresponding fiber-to-fiber bonding. R_{eff} is calculated as the hole radius where the models produce the mean measured unnotched tensile strength σ_M. As such, R_{eff} is

considered to be the size of the inherent defect in the material. Using a fracture mechanics approach, Donner[32] determined the defects in two newsprint samples (a short-fiber material) to range from 0.5 to 0.9 mm in the 1-direction and 1.2 to 1.7 mm in the 2-direction. These ranges are about twice the ranges observed for R_{eff} in Table 3 for papers that are made, for the most part, from long-fiber material.

The physical presence of a defect with a radius R_{eff} is unlikely. Rather, the inherent defect size accounts for innate interactions in the material during testing. Defects tend to interact with each other, producing lower or higher stresses than would be experienced independently. The combination of size and location of defects has not been thoroughly investigated except in special cases.[33]

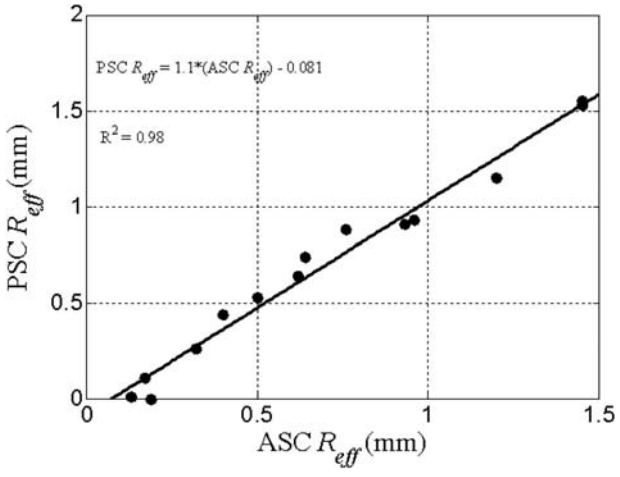

Figure 10. Relationship between ASC and PSC defect calculations.

Because both models, PSC and ASC, are based on the same stress distribution near the hole, Equation (1), the calculated defect sizes for each model are related to each other. Figure 10 shows the linear relationship between the R_{eff} values for PSC and ASC. For $R_{\text{eff}} < 0.81$ mm, PSC predicts a smaller R_{eff} than does ASC. The modified ASC is more reliable during regression, is less sensitive to initial parameter estimates, and calculates a finite-sized inherent defect, even as $R_{\text{eff}} \to 0$.

Figures 3–9 demonstrate the difficulty in application of Equations (7) and (8) to experimental strength data of materials with unknown defects, namely that by introducing a defect similar in size to the inherent defect, some failures will occur away from the introduced defect. Results of those tests were not included in the regression, thereby effectively adding statistical weight to results of the large hole strength data and reducing the effect of results near the region of interest (i.e., the smaller defects). To improve accuracy near the region of interest, for situations when the entire group of specimens failed away from the introduced defect, the standard binomial statistical-hypothesis test was used to test the hypothesis: *tensile specimens fail at the largest inherent defect*.

As stated earlier, the strength-controlling defect may be introduced, such as by hole punching, or it may be inherently part of the material. The standard binomial statistical-hypothesis test was used to determine the likelihood that the experimental strength would be above or equal to the model (either PSC or ASC). For the five replicates used in this study, only when all five specimens with the same introduced defect had strengths below the predicted (PSC or ASC) model

Table 4. Adjusted values for R_{eff} based on binomial statistical hypothesis test

		Point stress		Average stress	
Material	Direction	R_{eff} (mm)	Adjusted R_{eff} (mm)	R_{eff} (mm)	Adjusted R_{eff} (mm)
E	2	0.93	0.88	0.99	0.95
L1	2	1.53	1.63	1.49	1.60
L2	1	0.88	0.87	0.76	0.75
	2	1.55	1.56	1.45	1.46
S1	1	0.64	0.66	0.62	0.63
	2	0.91	0.82	0.97	0.89
S2	1	0.74	0.73	0.64	0.63
	2	1.15	1.10	1.20	1.16

Note: E, Envelope; L1, linerboard1; L2, linerboard2; S1, cylinder board1; and S2, cylinder board2. Only samples that are statistically significant are shown. Values for R_{eff} are from Table 3.

would the one-sided alternative be significant at the 5% level, according to the two-sided table in Snedecor and Cochrane.[34] Such a result would violate the statistical rules of chance. For this study, the binomial hypothesis test indicated that the following materials failed at inherent defects that were larger than the smallest (0.25 mm) defect: E (2-direction), L1 (2-direction), L2 (both directions), S1 (both directions), and S2 (both directions).

For these eight cases, the strength data at 0.25 mm introduced defect can be moved to the R_{eff} for the particular sample and maintain variability of the model. These additional data were used to determine an adjusted R_{eff}. Table 4 gives the adjusted R_{eff} for samples in those eight cases. Adjusted R_{eff} was greater than original R_{eff} for Materials L1 (2-direction), L2 (2-direction), and S1 (1-direction) because the mean tensile strength of specimens with 0.25 mm defect was greater than for the unnotched specimen. All other adjusted R_{eff} values were less than original R_{eff}. Application of the binomial statistical hypothesis test changed R_{eff} in a manner expected from graphical observation.

Conclusion

The classical PSC and ASC have been modified to determine inherent defect size R_{eff} and maximum potential tensile strength σ_{u} for seven cellulose fiber materials. Calculated defect sizes were well related to observations during tensile testing relating to location of failure in that failure away from the introduced defect indicated an inherent defect larger than the introduced hole. As expected, printing and writing grade papers exhibit the smallest size defects. The models are effective for a wide range of material weights and two manufacturing methods. The modified ASC model had more rapid parameter convergence than the modified PSC model and calculated a finite-sized defect for all materials. Data were well characterized by the modified PSC and modified ASC even though these theories are strictly valid only for linear elastic materials.

The binomial hypothesis test was used to determine cases where the inherent defect size analysis could be adjusted. The adjustment produced changes in accordance with observed data trends.

Because defect-free samples are the exception, the present approach extends the PSC and ASC in a manner beneficial for real-world situations. For the materials studied here, 30 tensile tests were sufficient for defect size and maximum potential tensile strength determination in one of the directions of orthotropy. Papermakers may use this approach to determine the favorable effect on strength of improving formation for cost-benefit analysis.

References

1. Miettinen PPJ, Ketoja JA and Hjelt T. Simulated structure of wet fiber networks. *Nord Pulp Pap Res J* 2007; 22(4): 516–522.
2. Rigdahl M, Andersson H, Westerlind B and Hollmark H. Elastic behavior of low-density paper described by network mechanics. *Fibre Sci Technol* 1983; 19(2): 127–144.
3. Astrom J, Saarinen S, Niskanen K and Kurkijarvi J. Microscopic mechanics of fiber networks. *J Appl Phys* 1994; 75(5): 2383–2392.
4. Norman RJ. Dependence of sheet properties on formation and forming variables. In: Bolam F (ed.) *Consolidation of the paper web, transactions of the IIIrd fundamental research symposium*. Cambridge. Manchester, UK: FRC, 1965, pp.269–298.
5. Moffatt J, Beath L and Mihelich W. Major factors in newsprint strength. In: Bolam F (ed.) *The fundamental properties of paper related to its uses, transactions of the Vth fundamental research symposium*, Cambridge. Manchester, UK: FRC, 1973, pp.104–127.
6. Nazhad MM, Harris EJ, Dodson CTJ and Kerekes RJ. The influence of formation on tensile strength of papers made from mechanical pulps. *Tappi J* 2000; 83(12): 63–63.
7. Nazhad MM, Karnchanapoo W and Palokangas A. Some effects of fibre properties on formation and strength of paper. *Appita J* 2003; 56(1): 61–65.
8. Mohlin UB. Fiber dimensions: Formation and strength. *Nord Pulp Pap Res J* 2001; 16(3): 235–239.
9. Nordstrom B. Effects of grammage on sheet properties in one-sided and two-sided roll forming. *Nord Pulp Pap Res J* 2003; 18(3): 280–287.
10. Wathen R and Niskanen K. Strength distributions of running paper webs. *J Pulp Pap Sci* 2006; 32(3): 137–144.
11. I'Anson SJ and Sampson WW. Competing Weibull and stress-transfer influences on the specific tensile strength of a bonded fibrous network. *Compos Sci Technol* 2007; 67(7–8): 1650–1658.
12. Suknyov SV. Estimation of the tensile strength reduction of a composite laminate with a hole. *Mech Compos Mater* 2000; 36(6): 439–444.
13. Korteoja MJ, Lukkarinen A, Kaski K, Gunderson DE, Dahlke JL and Niskanen KJ. Local strain fields in paper. *Tappi J* 1996; 79(4): 217–223.
14. Korteoja MJ, Lukkarinen A, Kaski K and Niskanen KJ. Computational study of formation effects on paper strength. *J Pulp Pap Sci* 1997; 23(1): J18–J22.
15. Choi D, Thorpe JL and Hanna RB. Image-analysis to measure strain in wood and paper. *Wood Sci. Technol* 1991; 25(4): 251–262.
16. Um GJ and Perkins RW. Stress and strain for perforated tensile specimens, part 1: Experimental measurements. *Tappi J* 2007; 6(3): 3–7.
17. Wong L, Kortschot MT and Dodson CTJ. Effect of formation on local strain fields and fracture of paper. *J Pulp Pap Sci* 1996; 22(6): J213–J219.
18. Considine JM, Scott CT, Gleisner R and Zhu JY. Use of digital image correlation to study the local deformation field of paper and paperboard. In: I'Anson SJ (ed.)

Advances in Paper Science and Technology, Transactions of the 13th Fundamental Research Symposium, Cambridge, September 2005 Bury, UK: The Pulp and Paper Fundamental Research Society, pp.613–630.
19. Hristopulos DT and Uesaka T. Structural disorder effects on the tensile strength distribution of heterogeneous brittle materials with emphasis on fiber networks. *Phys Rev B* 2004; 70(6): 064108.
20. Ostoja-Starzewski M and Castro J. Random formation, inelastic response and scale effects in paper. *Philos Trans R Soc A: Math Phys Eng Sci* 2003; 361(1806): 965–985.
21. Korteoja M, Salminen LI, Niskanen KJ and Alava M. Statistical variation of paper strength. *J Pulp Pap Sci* 1998; 24(1): 1–7.
22. Rhee J, Cho H, Marr D and Rowlands R. On local compliance, stress concentration and strength in orthtropic materials. In: *Society of Experimental Mechanics Conference*, Portland, OR, June, 2005.
23. Perkins RW and Um GJ. Stress and strain for perforated tensile specimens, part 2: FEA simulations. *Tappi J* 2007; 6(4): 22–27.
24. Kortschot MT and Trakas K. Predicting the strength of paper containing holes or cracks with the point stress criterion. *Tappi J* 1998; 81(1): 254–259.
25. Awerbuch J and Madhukar MS. Notched strength of composite laminates: Predictions and experiments - a review. *J Reinf Plast Compos* 1985; 4(1): 3–159.
26. Whitney JM and Nuismer RJ. Stress fracture criteria for laminated composites containing stress-concentrations. *J Compos Mater* 1974; 8(July): 253–265.
27. Lekhnitskii S. *Theory of elasticity of an anisotropic elastic body*. San Francisco, CA: Holden-Day, 1963.
28. Beyer WH. and Chemical Rubber Company. *CRC standard mathematical tables*. Boca Raton, FL: CRC Press, 1987.
29. Khashaba UA. Fracture behavior of woven composites containing various cracks geometry. *J Compos Mater* 2003; 37(1): 5–20.
30. Tan SC. Finite-width correction factors for anisotropic plate containing a central opening. *J Compos Mater* 1988; 22(11): 1080–1097.
31. McNulty JC, Zok FW, Genin GM and Evans AG. Notch-sensitivity of fiber-reinforced ceramic-matrix composites: Effects of inelastic straining and volume-dependent strength. *J Am Ceram Soc* 1999; 82(5): 1217–1228.
32. Donner BC. An heuristic model of paper rupture. In: *Proceedings of fundamentals of papermaking materials - 11th fundamental research symposium*. Pira International, Pulp and Paper Fundamental Research Society, Surrey, UK: Fundamental Research Committee, 1997, pp. 1215–1247.
33. Considine J, Vahey D, Skye W, Chen W, Turner K and Rowlands R. Shielding: new insight to the relationship between formation and strength. In: *Proceedings, PaperCon'09 TAPPI/Pima paper conference and trade show*, May 31–June 3, 2009, Saint Louis, MO, USA, p. Poster.
34. Snedecor GW and Cochran WG. *Statistical methods*. Ames, Iowa: Iowa State University Press, 1980.